Preprints (www.preprints.org) | NOT PEER-REVIEWED | Posted: 19 December 2018 doi:10.20944/preprints201812.0229.v1

Peer-reviewed version available at *Photonics* **2019**, *6*, 8; doi:10.3390/photonics6010008

Article

Holography Using Curved Metasurfaces

James Burch [1*], Andrea Di Falco [2]

[1] University of St Andrews; jb298@st-andrews.ac.uk
[2] University of St Andrews; adf10@st-andrews.ac.uk
* Correspondence: jb298@st-andrews.ac.uk; adf10@st-andrews.ac.uk; Tel.: +44 (0)1334 463165

Version December 19, 2018 submitted to Preprints

Abstract: In this work we demonstrate non-flat metasurface holograms with applications in imaging, sensing, and anti-counterfeiting. In these holograms the image and its symmetry properties, with respect to the polarization of the light, depend on the specific shape of the substrate. Additionally, the sensitivity of the holographic image to the substrate shape can be engineered by distributing the phase information into determined areas of the metasurface.

Keywords: Metasurfaces; holography; curved; metamaterials; non flat optics; tunable; reconfigurable

1. Introduction

Photonic metasurface (MS) are one of the most successful platforms to realize computer-generated holograms. These devices utilize sub-wavelength pixels to create holographic images with high efficiency [1–5]. Holographic MS enable the multiplexing of information in various degrees of freedom, including for example wavelength [6,7], angle [8], polarization [9–13], and image dimensionality [14]. Applications of MSs include the manipulation and storage of information [15,16], security [10], and displays [17].

MSs offer the possibility to modulate the amplitude and phase of light with high resolution and negligible thickness. These properties make MSs easily exploitable in flexible designs. Examples of these applications include cloaking, lab-on-fiber, optically active, and filtering devices [18–23].

Flexibility has been previously exploited for MS holograms in devices controlled by the degree of substrate stretching, e.g. to vary the focus of a MS lens [24], or to alternate between multiple near-field images [25]. A theoretical exploration of flexible MS holograms has also enabled carpet cloaking, and spherical aberration correction for lensing applications [26]. Flexible MSs have also been used to decouple the shape of a lens from its optical function [27].

Traditional flat MS holograms produce identical holographic images when illuminated by left- (LCP) and right-handed circularly polarized light (RCP) but with the holographic image rotated 180 degrees around the zeroth order of the beam [10]. In this work we demonstrate that for non-flat MSs both the shape of the substrate and the polarization of the incident light contribute to determine the symmetry properties of the image. Here we also describe how the sensitivity to the MSs shape can be tailored to provide versatility for practical applications including in anti-counterfeiting and surface topology sensing.

Rayleigh-Sommerfeld light propagation

We designed our holograms using the Gerchberg-Saxton iterative phase reconstruction algorithm. To describe the general case of propagation between the non-flat MS and the image planes we adopted the full Rayleigh-Sommerfeld propagation method [28], as given by

$$U(x_I, y_I, z_I) = -\iint U(x_O, y_O, z_O)\frac{2(z_I - z_O)}{|\mathbf{r}_I - \mathbf{r}_O|} \times (ik - \frac{1}{|\mathbf{r}_I - \mathbf{r}_O|}) \times \frac{\exp(ik|\mathbf{r}_I - \mathbf{r}_O|)}{4\pi|\mathbf{r}_I - \mathbf{r}_O|}\, dx_O\, dy_O. \tag{1}$$

© 2018 by the author(s). Distributed under a Creative Commons CC BY license.

Preprints (www.preprints.org) | NOT PEER-REVIEWED | Posted: 19 December 2018 doi:10.20944/preprints201812.0229.v1

Peer-reviewed version available at Photonics 2019, 6, 8; doi:10.3390/photonics6010008

where the cartesian coordinates (x_j, y_j, z_j) relate to the position vectors $\mathbf{r}_j$, U is the complex light field, k is the wavevector of light, and the holographic MS object and imaging planes are denoted with the subscripts $j = O, I$ respectively. Here the coordinate system is aligned to the center of the undistorted MS. An illustration of this method can be seen in figure 1.

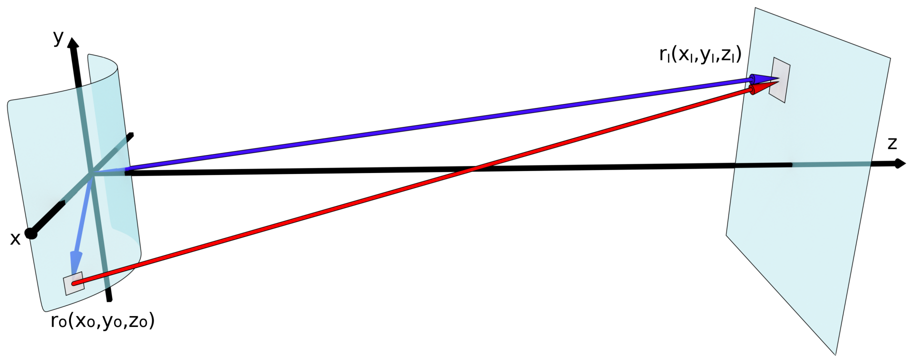

Figure 1. Light propagation from $\mathbf{r}_O(x_O, y_O, z_O)$ to $\mathbf{r}_I(x_I, y_I, z_I)$ using the Rayleigh-Sommerfeld equation. The holographic image originates from the MS and is projected onto the screen.

For flat MS, inverting the handedness of the polarization, for example from RCP to LCP, typically creates a holographic image rotated by 180 degrees around the zeroth order of the holographic image [10]. This occurs because each Pancharatnam-Berry element provides the same de-phasing, but with an opposite sign between the two polarizations $\phi_0(x_O, y_O, z_O) \rightarrow -\phi_0(x_O, y_O, z_O)$ [1,29]. With more complex meta-atoms a similar effect can be used to encode entirely different holographic images [30,31].

The rotation of the holographic image around the zeroth order can be described through the equation

$$I'(x_I, y_I) = I(-x_I, -y_I) \tag{2}$$

where I' and I are the intensity distributions in the holographic image plane for the rotated and non rotated holographic images respectively. x_I and y_I refer to the position in the holographic image plane in the x and y directions respectively, and the z coordinate is constant.

For the non-flat MS case, equation 2 only holds true when both the phase contribution from the polarization $\phi_0(x_O, y_O, z_O) \rightarrow -\phi_0(x_O, y_O, z_O)$, and the phase contribution from the MS shape $\phi_c(x_O, y_O, z_O) \rightarrow -\phi_c(x_O, y_O, z_O)$ are both inverted [32].

As such, equation 2 for the non-flat MS case is true when

$$\phi_c(x_O, y_O, z_O) + \phi_0(x_O, y_O, z_O) \rightarrow -\phi_c(x_O, y_O, z_O) - \phi_0(x_O, y_O, z_O) \tag{3}$$

Conversely, for a flat MS the phase contribution $\phi_c(x_O, y_O, z_O)$ is necessarily 0 and changing the handedness of the polarization leads to the rotation of the holographic image by 180 degrees.

Results and discussion

When we design non-flat MS holograms using the Gerchberg-Saxton algorithm, the recovered phase holograms are specific to the surface profile. Changing the MS shape will then result in a distorted holographic image. Our chosen holographic MS design uses as Pancharatnam-Berry de-phasing elements a regular array of gold nanorods, sitting on a polymeric spacing layer deposited on a reflective gold backplane [32,33]. Each unit cell, comprising a nanorod separated by the thin

Preprints (www.preprints.org) | NOT PEER-REVIEWED | Posted: 19 December 2018 doi:10.20944/preprints201812.0229.v1

Peer-reviewed version available at *Photonics* **2019**, *6*, 8; doi:10.3390/photonics6010008

dielectric layer from the gold backplane, can be approximated as an isotropically emitting Huygen's source. This three-layer structure is realized on a free-standing and flexible 2 μm thick polymeric membrane. To define the nanorods on the top surface we used a standard electron beam lithography procedure [33] followed by dry back etching of the unmasked superficial gold layer. The quality of the MS after lift-off is illustrated in figure 2(a) with an SEM image. Figure 2(b) shows a typical flexible holographic MS applied to a non-flat surface.

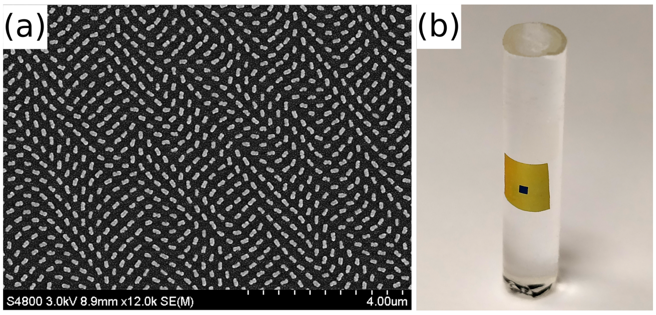

Figure 2. (a) The nanorods comprising the MS and imaged with an SEM after the membrane was lifted from the rigid initial substrate. (b) An experimental image displaying a MS conformed to a non-flat surface. The MS itself can be seen as the green square central on the gold membrane.

As described through equations 1-2, to obtain a correctly rotated holographic image it is necessary to change the symmetry of the substrate with respect to the xy plane (e.g. change z into -z), as well as the handedness of the polarization. The experimental demonstration of this statement is displayed in figure 3.

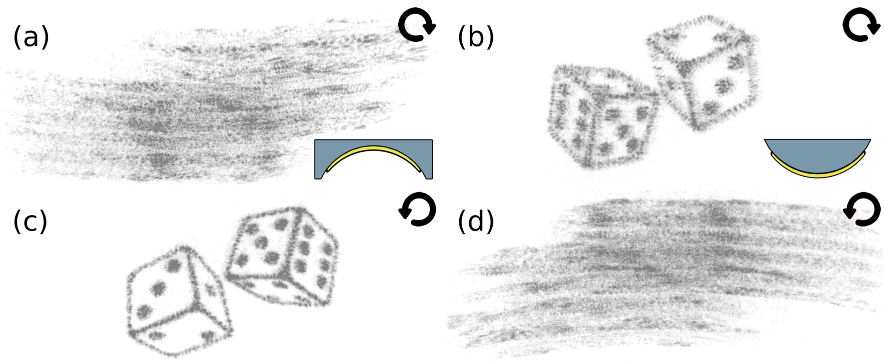

Figure 3. Experimental holographic images where (a,b) and (c,d) were illuminated with right handed, and left handed circular polarizations respectively. (a,c) used a concave substrate with a radius of curvature of 6 mm, (b,d) used a convex substrate with the same radius of curvature. The LCP images are rotated 180 degrees in the holographic image plane compared to the RCP images.

To evaluate the specificity of the holographic image to a particular substrate shape we designed and fabricated holographic MS for a flat surface, and convex cylinders with radii of curvature of 6 mm and 4 mm. We then compared the images obtained by these three MSs when applied to a cylinder with a radius of curvature of 6 mm. As can be seen in figure 4 the agreement between simulation and experiment is good. The greater the disparity between the surface shape that the MS hologram was designed for and the actual MS shape, the greater the distortion of the holographic image. A quantitative analysis of the distortion of the images was completed by evaluating the correlation coefficient of the simulated holographic images compared to the ideal target image. Here a correlation coefficient of 1 means that the two images are identical, and a coefficient close to 0 means no correlation. Even in simulation we do not expect a correlation coefficient of 1 because the number of iterations we perform during the phase retrieval is finite, and because we are encoding only the phase and not the amplitude information into the MS. Our analysis, as seen in the numbers in figure 4, demonstrates that

Preprints (www.preprints.org) | NOT PEER-REVIEWED | Posted: 19 December 2018 doi:10.20944/preprints201812.0229.v1

Peer-reviewed version available at Photonics 2019, 6, 8; doi:10.3390/photonics6010008

the correlation coefficient for holographic images where the MS has the correct surface shape is close to 1, but that the correlation coefficient drops to below half of this value when the MS has the incorrect shape [32].

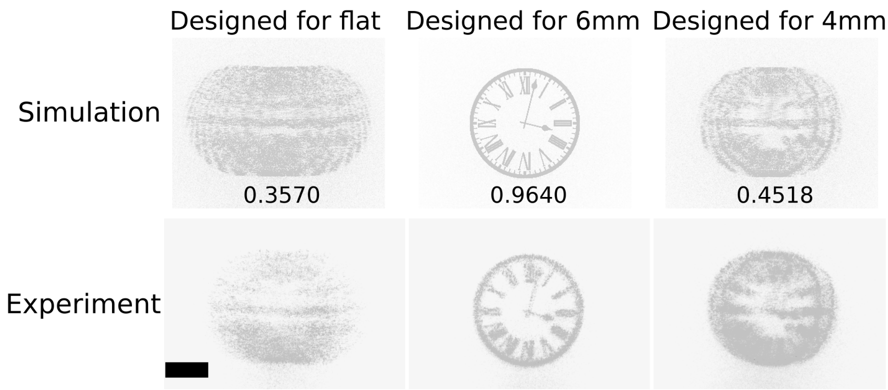

Figure 4. Simulated and experimental holographic image results, comparing MS designed for various convex cylinders with differing radii of curvature. In each case the MS was analyzed as being applied to a convex cylinder with a radius of curvature of 6 mm. For the experimental results the scale bar represents 10 mm. The numbers correspond to the correlation coefficient where 1 is perfect correlation.

The sensitivity of the MS holograms to the surface shape can also be increased by carefully distributing the holographic phase information in the MS. For the specific example of cylindrical substrates with different radii of curvature, the gradient and position of the phase elements in the central region along the long axis of the cylinder are changed the least. As shown in detail in ref. [32], MSs with no phase information encoded in the central region maintained the peak holographic image quality, while increasing their sensitivity to the MS shape.

2. Materials and Methods

To fabricate our samples we first spin coat a polymeric sacrificial layer onto a silicon substrate. Next we spin a 2 μm thick polymer (SU-8, Microchem) on top, which acts as flexible substrate. Next we deposit a 100 nm thick layer of gold to act as a backplane mirror. Next we spin on another layer of SU-8 with a thickness of 90 nm and crosslink it with a flood UV exposure. Next we deposit an additional 40 nm of gold for the nanorods. Next we spin on another layer of SU-8 with a thickness of 90 nm as an electron beam resist. Next we pattern the nanorod using a top-down standard electron beam lithography approach. Next we use a reactive ion etch to remove unmasked gold. Lastly we remove the sacrificial layer to leave a free-floating membrane.

3. Conclusions

We demonstrate a holographic MS where the holographic image has a strong dependence on the MS shape. Next, we describe the additional symmetry condition that MS Pancharatnam-Berry holograms exhibit compared to their flat counterparts. We also show how the holographic information in the MS can be encoded to tailor the sensitivity of the resulting holographic image to the MS shape. This work could be applied in fields ranging from sensors to anti-counterfeiting devices and lenses.

4. Patents

Holographic device patent application. UK patent application number GB1719588.4.

Author Contributions: J.B. designed, fabricated and characterized the MSs. Both authors wrote the manuscript. ADF directed the project.

Acknowledgments: J.B. and A.D.F. acknowledge support from EPSRC (Grant Nos. EP/M508214/1 and EP/L017008/1). The research data supporting this publication can be accessed at http://dx.doi.org/10.17630/583a258e-32cb-4a6b-826c- ab7d3b4429e2.

Preprints (www.preprints.org) | NOT PEER-REVIEWED | Posted: 19 December 2018 doi:10.20944/preprints201812.0229.v1

Peer-reviewed version available at Photonics 2019, 6, 8; doi:10.3390/photonics6010008

Conflicts of Interest: The authors declare no conflict of interest.

References

1. Zheng, G.; Mühlenbernd, H.; Kenney, M.; Li, G.; Zentgraf, T.; Zhang, S. Metasurface holograms reaching 80% efficiency. *Nature Nanotechnology* **2015**, *10*, 308–312.
2. Arbabi, A.; Horie, Y.; Ball, A.; Bagheri, M.; Faraon, A. Subwavelength-thick lenses with high numerical apertures and large efficiency based on high-contrast transmitarrays. *Nature Communications* **2015**, *6*, 7069.
3. Arbabi, A.; Horie, Y.; Bagheri, M.; Faraon, A. Dielectric metasurfaces for complete control of phase and polarization with subwavelength spatial resolution and high transmission. *Nature Nanotechnology* **2015**, *10*, 937–943.
4. Wei, Z.; Cao, Y.; Su, X.; Gong, Z.; Long, Y.; Li, H. Highly efficient beam steering with a transparent metasurface. *Optics Express* **2013**, *21*, 10739–10745.
5. Wang, L.; Kruk, S.; Tang, H.; Li, T.; Kravchenko, I.; Neshev, D.N.; Kivshar, Y.S. Grayscale transparent metasurface holograms. *Optica* **2016**, *3*, 1504–1505.
6. Montelongo, Y.; Tenorio-Pearl, J.O.; Williams, C.; Zhang, S.; Milne, W.I.; Wilkinson, T.D. Plasmonic nanoparticle scattering for color holograms. *Proceedings of the National Academy of Sciences* **2014**, *111*, 12679–12683.
7. Li, X.; Chen, L.; Li, Y.; Zhang, X.; Pu, M.; Zhao, Z.; Ma, X.; Wang, Y.; Hong, M.; Luo, X. Multicolor 3D meta-holography by broadband plasmonic modulation. *Science Advances* **2016**, *2*, e1601102.
8. Kamali, S.M.; Arbabi, E.; Arbabi, A.; Horie, Y.; Faraji-Dana, M.; Faraon, A. Angle-multiplexed metasurfaces: encoding independent wavefronts in a single metasurface under different illumination angles. *Phys Rev X* **2017**, *7*, 041056.
9. Liu, H.C.; Yang, B.; Guo, Q.; Shi, J.; Guan, C.; Zheng, G.; Mühlenbernd, H.; Li, G.; Zentgraf, T.; Zhang, S. Single-pixel computational ghost imaging with helicity-dependent metasurface hologram. *Science Advances* **2017**, *3*, e1701477.
10. Wen, D.; Yue, F.; Li, G.; Zheng, G.; Chan, K.; Chen, S.; Chen, M.; Li, K.F.; Wong, P.W.H.; Cheah, K.W.; Pun, E.Y.B.; Zhang, S.; Chen, X. Helicity multiplexed broadband metasurface holograms. *Nature Communications* **2015**, *6*, 8241.
11. Montelongo, Y.; Tenorio-Pearl, J.; Milne, W.; Wilkinson, T. Polarization switchable diffraction based on subwavelength plasmonic nanoantennas. *Nano Letters* **2013**, *14*, 294–298.
12. Ye, W.; Zeuner, F.; Li, X.; Reineke, B.; He, S.; Qiu, C.W.; Liu, J.; Wang, Y.; Zhang, S.; Zentgraf, T. Spin and wavelength multiplexed nonlinear metasurface holography. *Nature Communications* **2016**, *7*, 11930.
13. Khorasaninejad, M.; Ambrosio, A.; Kanhaiya, P.; Capasso, F. Broadband and chiral binary dielectric meta-holograms. *Science Advances* **2016**, *2*, e1501258.
14. Huang, L.; Mühlenbernd, H.; Li, X.; Song, X.; Bai, B.; Wang, Y.; Zentgraf, T. Broadband hybrid holographic multiplexing with geometric metasurfaces. *Advanced Materials* **2015**, *27*, 6444–6449.
15. Nobukawa, T.; Nomura, T. Multilayer recording holographic data storage using a varifocal lens generated with a kinoform. *Optics Letters* **2015**, *40*, 5419–5422.
16. Shimada, K.i.; Ide, T.; Shimano, T.; Anderson, K.; Curtis, K. New optical architecture for holographic data storage system compatible with Blu-ray Disc^{TM} system. *Optical Engineering* **2014**, *53*, 025102–025102.
17. Huang, L.; Chen, X.; Mühlenbernd, H.; Zhang, H.; Chen, S.; Bai, B.; Tan, Q.; Jin, G.; Cheah, K.W.; Qiu, C.W.; Li, J.; Zentgraf, T.; Zhang, S. Three-dimensional optical holography using a plasmonic metasurface. *Nature Communications* **2013**, *4*, 2808.
18. Di Falco, A.; Ploschner, M.; Krauss, T. Flexible metamaterials at visible wavelengths. *New Journal of Physics* **2010**, *12*, 113006.
19. Reader-Harris, P.; Di Falco, A. Nanoplasmonic filters for hollow core photonic crystal fibers. *ACS Photonics* **2014**, *1*, 985–989.
20. Reader-Harris, P.; Ricciardi, A.; Krauss, T.; Di Falco, A. Optical guided mode resonance filter on a flexible substrate. *Optics Express* **2013**, *21*, 1002–1007.
21. Di Falco, A.; Zhao, Y.; Alú, A. Optical metasurfaces with robust angular response on flexible substrates. *Applied Physics Letters* **2011**, *99*, 163110.

Preprints (www.preprints.org) | NOT PEER-REVIEWED | Posted: 19 December 2018 doi:10.20944/preprints201812.0229.v1

Peer-reviewed version available at *Photonics* **2019**, *6*, 8; doi:10.3390/photonics6010008

22. Yang, S.; Liu, P.; Yang, M.; Wang, Q.; Song, J.; Dong, L. From flexible and stretchable meta-atom to metamaterial: A wearable microwave meta-skin with tunable frequency selective and cloaking effects. *Scientific Reports* **2016**, *6*, 21921.
23. Walia, S.; Shah, C.; Gutruf, P.; Nili, H.; Chowdhury, D.R.; Withayachumnankul, W.; Bhaskaran, M.; Sriram, S. Flexible metasurfaces and metamaterials: A review of materials and fabrication processes at micro-and nano-scales. *Applied Physics Reviews* **2015**, *2*, 011303.
24. Ee, H.S.; Agarwal, R. Tunable metasurface and flat optical zoom lens on a stretchable substrate. *Nano Letters* **2016**, *16*, 2818–2823.
25. Malek, S.C.; Ee, H.S.; Agarwal, R. Strain multiplexed metasurface holograms on a stretchable substrate. *Nano Letters* **2017**, *17*, 3641–3645.
26. Cheng, J.; Jafar-Zanjani, S.; Mosallaei, H. All-dielectric ultrathin conformal metasurfaces: lensing and cloaking applications at 532 nm wavelength. *Scientific Reports* **2016**, *6*, 38440.
27. Kamali, S.M.; Arbabi, A.; Arbabi, E.; Horie, Y.; Faraon, A. Decoupling optical function and geometrical form using conformal flexible dielectric metasurfaces. *Nature communications* **2016**, *7*, 11618.
28. Veerman, J.A.; Rusch, J.J.; Urbach, H.P. Calculation of the Rayleigh–Sommerfeld diffraction integral by exact integration of the fast oscillating factor. *JOSA A* **2005**, *22*, 636–646.
29. Huang, Y.W.; Chen, W.T.; Tsai, W.Y.; Wu, P.C.; Wang, C.M.; Sun, G.; Tsai, D.P. Aluminum plasmonic multicolor meta-hologram. *Nano Letters* **2015**, *15*, 3122–3127.
30. Mueller, B.; Rubin, N.; Devlin, R.; Groever, B.; Capasso, F. Metasurface Polarization Optics: Independent Phase Control of Arbitrary Orthogonal States of Polarization. *Physical Review Letters* **2017**, *118*, 113901.
31. Wen, D.; Chen, S.; Yue, F.; Chan, K.; Chen, M.; Ardron, M.; Li, K.F.; Wong, P.W.H.; Cheah, K.W.; Pun, E.Y.B.; Li, G.; Zhang, S.; Chen, X. Metasurface Device with Helicity-Dependent Functionality. *Advanced Optical Materials* **2016**, *4*, 321–327.
32. Burch, J.; Di Falco, A. Surface topology specific metasurface holograms. *ACS Photonics* **2018**, *5*, 1762–1766.
33. Burch, J.; Wen, D.; Xianzhong, C.; Di Falco, A. Conformable Holographic Metasurfaces. *Scientific Reports* **2017**, *7*, 4520.